Draft version October 16, 2015
Preprint typeset using LaTeX style emulateapj v. 5/2/11

arXiv:1510.04451v1 [astro-ph.SR] 15 Oct 2015

UPDATED 24 μM PERIOD-LUMINOSITY RELATION DERIVED FROM GALACTIC CEPHEIDS

Chow-Choong Ngeow[1], Saurjya Sarkar[2], Anupam Bhardwaj[3], Shashi M. Kanbur[4] and Harinder P. Singh[3]

Draft version October 16, 2015

ABSTRACT

In this work, we updated the catalog of Galactic Cepheids with 24μm photometry by cross-matching the positions of known Galactic Cepheids to the recently released MIPSGAL point source catalog. We have added 36 new sources featuring MIPSGAL photometry in our analysis, thus increasing the existing sample to 65. Six different sources of compiled Cepheid distances were used to establish a 24μm period-luminosity (P-L) relation. Our recommended 24μm P-L relation is $M_{24\mu\mathrm{m}} = -3.18(\pm0.10)\log P - 2.46(\pm0.10)$, with an estimated intrinsic dispersion of 0.20 mag, and is derived from 58 Cepheids exhibiting distances based on a calibrated Wesenheit function. The slopes of the P-L relations were steepest when tied solely to the 10 Cepheids exhibiting trigonometric parallaxes from the *Hubble Space Telescope* and *Hipparcos*. Statistical tests suggest that these P-L relations are significantly different from those associated with other methods of distance determination, and simulations indicate that difference may arise from the small sample size.

Subject headings: stars: variables: Cepheids — distance scale — stars: distances

1. INTRODUCTION

The Cepheid period-luminosity relation (P-L relation, also known as the Leavitt Law) for classical Cepheids (hereafter Cepheids) is an important astrophysical tool in distance scale studies that allows a determination of a Hubble's constant (for examples, see Freedman et al. 2001; Sandage et al. 2006; Riess et al. 2011) that is independent of the cosmic microwave background anisotropy measurements from *WMAP (Wilkinson Microwave Anisotropy Probe)* or *Planck*. A large number of papers on the calibrations and applications of the Cepheid P-L relation in the optical VI bands and near-infrared JHK bands can be found in the literature and will not be listed here.

In recent years, attention has turned to the mid-infrared Cepheid P-L relations based on the *Spitzer's* IRAC bands in 3.6, 4.5, 5.8 and 8.0 μm bands. The advantages of applying these mid-infrared P-L relations instead of their shorter wavelength counterparts include smaller amplitudes of the light curves, a smaller dispersion on the P-L relations[5], and less sensitivity to extinction in the mid-infrared. The IRAC bands P-L relations have been derived for Cepheids in our Galaxy (Marengo et al. 2010; Monson et al. 2012; Ngeow 2012), the Large Magellanic Cloud (LMC; for example in Freedman et al. 2008; Ngeow & Kanbur 2008; Scowcroft et al. 2011), the Small Magellanic Cloud (SMC; Ngeow & Kanbur 2010; Ngeow et al. 2015), or in both Clouds (Majaess et al. 2013; Riebel et al. 2015). Theoretical investigation of the IRAC bands P-L relations can also be found in Ngeow et al. (2012a). Marengo et al. (2010) derived the first 24μm (and 70μm) P-L relation beyond 8.0μm, which was further refined by Ngeow (2012). Table 1 summarizes the available 24μm P-L relations based on 29 (or less) Galactic Cepheids with independent distances measured using various methods. It can be seen from this Table that the 24μm P-L relations given in Marengo et al. (2010) and Ngeow (2012) do not agree with each other. Additional Cepheids observed in the 24μm band with the latest distance calibration are needed to recalibrate the 24μm P-L relation.

The "24 and 70 Micron Survey of the Inner Galactic Disk with MIPS" program (abbreviated as the MIPSGAL; Carey et al. 2009) is a *Spitzer* Legacy Program that surveyed the inner Galactic Plane by using the Multiband Infrared Photometer for the *Spitzer* (MIPS) instrument (Rieke et al. 2004). Gutermuth & Heyer (2015) recently released a 24μm point source catalog based on MIPSGAL data. Therefore, the goal of this paper is to match the known Galactic Cepheids with the MIPSGAL point source catalog in order to increase the number of Galactic Cepheids with 24μm photometry, and hence improve the calibration of the 24μm P-L relation. The mid-infrared P-L relations will be important in the era of the *James Webb Space Telescope (JWST)*, as instruments on board the *JWST* will be mainly operated in the mid-infrared (for example, with the $F2550W$ filter installed on the Mid-Infrared Imager, also known as the MIRI; see Bouchet et al 2015; Rieke et al. 2015)[6], and hence extra-galactic Cepheids will be routinely observed by *JWST*. The data used in this work is described in Section 2. Analysis and calibration of the 24μm P-L relation will be presented in Section 3, followed by a discussion

[1] Graduate Institute of Astronomy, National Central University, Jhongli 32001, Taiwan
[2] Birla Institute of Technology and Science, Pilani, 333031, India
[3] Department of Physics & Astrophysics, University of Delhi, Delhi 110007, India
[4] Department of Physics, SUNY Oswego, Oswego, NY 13126, USA

[5] Note that the P-L relations here refer to single-band P-L relations. Some of the Wesenheit functions, which incorporate a color term, will have a dispersion comparable to or smaller than the single-band P-L relations in the mid-infrared (for example, see Ngeow 2012; Inno et al. 2013; Bhardwaj et al. 2015b).

[6] It is true that photometric transformation is needed to convert the photometry between *Spitzer*'s MIPS 24μm band and *JWST*'s MIRI 25.5μm band (the central wavelength of $F2550W$ filter), however, detailed investigation of such transformation is beyond the scope of this paper.

Table 1
A Summary of Currently Known 24μm P-L Relations.[a]

Reference	N	η	β	σ	Source of Distances and Note[b]
Marengo et al. (2010)	29	-3.67 ± 0.03	-2.11 ± 0.04	~ 0.2	"old" IRSB + astrometric
Marengo et al. (2010)	28	-3.52 ± 0.06	-2.19 ± 0.08	~ 0.2	"new" IRSB + astrometric
Marengo et al. (2010)	8	-3.51 ± 0.21	-2.24 ± 0.27	~ 0.2	astrometric
Ngeow (2012)	29	-3.34 ± 0.06	-2.42 ± 0.06	0.11	Wesenheit distance; include DCEPS Cepheids
Ngeow (2012)	24	-3.37 ± 0.05	-2.41 ± 0.06	0.09	Wesenheit distance; exclude DCEPS Cepheids

[a] The P-L relation takes the form of $M_{24\mu m} = \eta \log P + \beta$, and σ is the dispersion of the P-L relation. N is the number of Galactic Cepheids used to derive the corresponding P-L relation.
[b] Source of distances: see Marengo et al. (2010) for the meaning of "old" IRSB (infrared surface brightness method) distances, "new" IRSB distances, and astrometric distances; the Wesenheit distances given in Ngeow (2012) are based on a period-Wesenheit relation calibrated with parallaxes measured in Benedict et al. (2007).

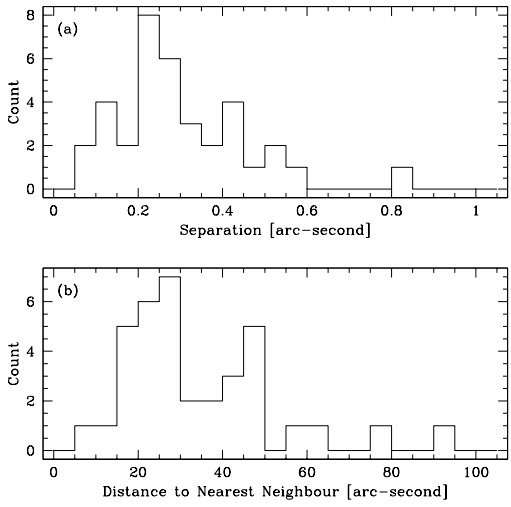

Figure 1. (a): Distribution of the separation (in arcsecond) between the input coordinates for Cepheids and the matched sources in the MIPSGAL catalog. The two Cepheids with largest separation are RU SCT (with 0.56 arcsec separation) and EZ CYG (with 0.81 arcsec separation). **(b):** Histogram of the distance (in arcsecond) to nearest neighbor for each of the matched sources as given in the MIPSGAL catalog. The two Cepheids with the shortest distance to their nearest neighbor are U Nor (8.7 arcsec away) and SU Cru (11.0 arcsec away).

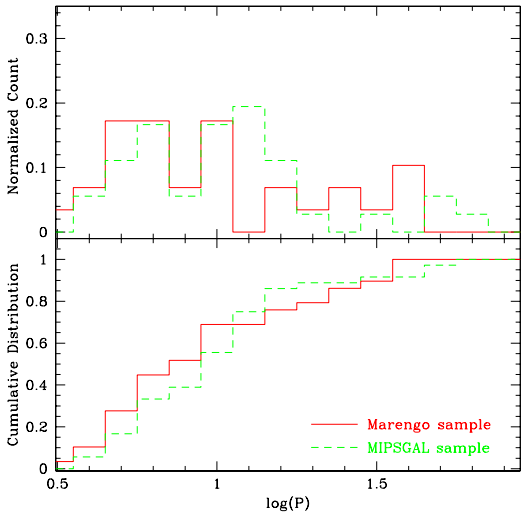

Figure 2. Histograms (upper panel) and cumulative distributions (lower panel) of the Marengo sample and the MIPSGAL sample.

and our conclusions in Section 4.

2. THE DATA

The positions of the Cepheids listed in Table 1 of Ngeow (2012) were cross-matched to the MIPSGAL Catalog[7] hosted at the NASA/IPAC Infrared Science Archive (IRSA). Since the pixel scale, in arcseconds, is 2.49×2.60 for MIPS at 24μm[8], we adopted a search radius of 2.6 arcsec. A total of 36 matched sources were returned. The number of matched sources does not increase even if we use a search radius of 10 arcsec. The top panel of Figure 1 displays the distribution of separations between these matched sources and the input locations. In all of the matched sources, the separations do not exceed 1 arcsec. The bottom panel of Figure 1 shows the histogram of the distances to the nearest neighbor for all of the matched sources returned from the query, which are all located at a distance that is more than two times of the searched radius. The 24μm photometry of the matched Cepheids from the MIPSGAL catalog is listed in Table 2, and is referred to as the MIPSGAL sample. Note that the brightest matched Cepheid has a 24μm magnitude of 2.47 ± 0.02 mag (i.e., X Sgr), which is fainter than the roughly estimated saturation limit at ~ 0 mag in the MIPSGAL catalog (for example, see Figure 8 in Gutermuth & Heyer 2015). Hence, none of our matched Cepheids suffered from the loss of fluxes due to saturation. For completeness, we also include the Cepheids from Marengo et al. (2010) in Table 2 as the Marengo sample. The 36 matched Cepheids in the MIPSGAL sample do not overlap with the Cepheids in the Marengo sample. Therefore, this increases the number of Galactic Cepheids with random phase 24μm photometry to 65 and represents the largest sample of Cepheids to date at this wavelength. Figure 2 presents the period distribution (upper panel) and the respective cumulative distribution (lower panel) for these two samples. The Kolmogorov-Smirnov (K-S) test returned a KS statistic of 0.217 and a p-value of 0.388 (which is larger than the adopted confidence level of $\alpha = 0.05$), and therefore the null hypothesis that these two samples were drawn from the same population cannot be rejected. Hereafter, we denoted the Marengo+MIPSGAL sample as the combined sample.

[7] http://irsa.ipac.caltech.edu/data/SPITZER/MIPSGAL/
[8] http://irsa.ipac.caltech.edu/data/SPITZER/docs/mips/mipsinstrumenthandbook/

Table 2
The 24μm Photometry and Distance Moduli for the Galactic Cepheids.[a]

name	Type	$\log P$	[24]	μ_{N12}	μ_{S11}	μ_{G13}	μ_{LKH}	μ_{noLKH}	μ_{B15}
				MIPS Sample					
CM SCT	DCEP	0.593	7.04 ± 0.10	11.58	···	···	···	···	···
EV SCT	DCEPS	0.643	6.50 ± 0.08	11.16	11.24 ± 0.10	···	···	···	11.23 ± 0.15
V0482 SCO	DCEP	0.656	5.26 ± 0.02	9.94	···	···	···	···	···
BR VUL	DCEP	0.716	6.82 ± 0.03	11.45	···	···	···	···	···
VW CRU	DCEP	0.722	5.79 ± 0.02	10.49	···	···	···	···	···
V0659 CEN	DCEP	0.750	4.61 ± 0.02	9.50	···	···	···	···	···
BB CEN	DCEPS	0.757	7.57 ± 0.16	12.29	···	···	···	···	···
V0773 SGR	DCEP	0.760	6.13 ± 0.03	10.39	···	···	···	···	···
FM AQL	DCEP	0.786	4.91 ± 0.02	9.74	10.36 ± 0.05	10.38 ± 0.09	···	···	10.36 ± 0.15
AD CRU	DCEP	0.806	7.52 ± 0.15	12.27	···	···	···	···	···
T CRU	DCEP	0.828	4.45 ± 0.02	9.52	···	···	···	···	···
X SGR	DCEP	0.846	2.47 ± 0.02	7.64	7.54 ± 0.04	7.51 ± 0.10	7.64 ± 0.13	7.61 ± 0.13	7.60 ± 0.10
CK SCT	DCEP	0.870	6.55 ± 0.05	11.51	···	11.86 ± 0.29	···	···	11.86 ± 0.23
U VUL	DCEP	0.903	3.77 ± 0.02	8.87	9.09 ± 0.04	9.07 ± 0.10	···	···	9.09 ± 0.15
V0378 CEN	DCEPS	0.969	5.75 ± 0.03	11.22	···	···	···	···	···
V0500 SCO	DCEP	0.969	5.20 ± 0.02	10.64	···	···	···	···	···
V0339 CEN	DCEP	0.976	5.62 ± 0.02	11.20	···	···	···	···	···
Y SCT	DCEP	1.015	5.28 ± 0.02	11.07	···	11.24 ± 0.15	···	···	11.24 ± 0.15
TW NOR	DCEP	1.033	6.50 ± 0.04	11.70	11.70 ± 0.10	11.80 ± 0.19	···	···	11.66 ± 0.19
TY SCT	DCEP	1.043	6.27 ± 0.07	11.86	···	11.51 ± 0.16	···	···	11.51 ± 0.15
EZ CYG	DCEP	1.067	7.42 ± 0.03	13.14	···	···	···	···	···
SY NOR	DCEP	1.102	5.63 ± 0.04	11.72	···	···	···	···	···
U NOR	DCEP	1.102	4.89 ± 0.02	10.73	10.55 ± 0.07	10.67 ± 0.07	···	···	10.55 ± 0.15
SU CRU	DCEP	1.109	4.46 ± 0.02	10.68	10.53 ± 0.15	···	···	···	10.53 ± 0.15
OO CEN	DCEP	1.110	6.81 ± 0.07	13.04	···	···	···	···	···
GX SGE	DCEP	1.111	7.22 ± 0.05	12.79	···	···	···	···	···
Z SCT	DCEP	1.111	6.11 ± 0.02	12.11	···	···	···	···	···
AV SGR	DCEP	1.188	5.39 ± 0.02	11.72	···	11.95 ± 0.18	···	···	···
V0470 SCO	DCEP	1.211	4.65 ± 0.02	10.57	···	···	···	···	···
TX CEN	DCEP	1.233	6.08 ± 0.03	12.32	···	···	···	···	···
QY CEN	DCEP	1.249	5.98 ± 0.06	12.28	···	···	···	···	···
RU SCT	DCEP	1.294	4.82 ± 0.04	11.32	11.39 ± 0.04	11.27 ± 0.07	···	···	11.34 ± 0.24
KQ SCO	DCEP	1.458	4.79 ± 0.04	11.76	12.23 ± 0.07	11.90 ± 0.09	···	···	12.25 ± 0.14
SV VUL	DCEP	1.653	3.83 ± 0.02	11.43	11.39 ± 0.02	11.69 ± 0.07	···	···	11.37 ± 0.14
GY SGE	DCEP	1.713	4.20 ± 0.02	11.71	12.29 ± 0.03	11.60 ± 0.65	···	···	12.37 ± 0.38
S VUL	DCEP	1.838	4.41 ± 0.02	12.54	12.88 ± 0.03	12.94 ± 0.11	···	···	12.81 ± 0.34
				Marengo Sample					
DT CYG	DCEPS	0.550	4.367 ± 0.002	8.74	8.97 ± 0.11	9.95 ± 0.43	8.75 ± 0.37	8.57 ± 0.37	8.97 ± 0.15
RT AUR	DCEP	0.572	3.773 ± 0.002	8.36	7.95 ± 0.02	8.38 ± 0.14	8.15 ± 0.17	8.10 ± 0.17	8.04 ± 0.14
BF OPH	DCEP	0.610	5.031 ± 0.005	9.51	9.25 ± 0.03	9.40 ± 0.10	···	···	9.25 ± 0.15
FF AQL	DCEP	0.650	3.338 ± 0.001	7.97	7.84 ± 0.06	9.12 ± 0.29	7.79 ± 0.14	7.76 ± 0.14	7.81 ± 0.10
SZ TAU	DCEPS	0.651	4.209 ± 0.002	8.73	8.73 ± 0.02	8.89 ± 0.10	···	···	8.73 ± 0.15
V0350 SGR	DCEP	0.712	5.032 ± 0.009	9.81	9.98 ± 0.05	9.81 ± 0.12	···	···	9.98 ± 0.15
δ CEP	DCEP	0.730	2.120 ± 0.001	7.09	7.13 ± 0.04	6.99 ± 0.15	7.19 ± 0.09	7.18 ± 0.09	7.15 ± 0.28
V CEN	DCEP	0.740	4.424 ± 0.003	9.27	9.04 ± 0.07	9.21 ± 0.08	···	···	9.08 ± 0.20
α UMi	DCEPS	0.754	0.723 ± 0.001	5.57	···	···	5.61 ± 0.03	5.61 ± 0.03	···
BB SGR	DCEP	0.822	4.339 ± 0.004	9.45	9.69 ± 0.03	9.55 ± 0.08	···	···	9.58 ± 0.51
U SGR	DCEP	0.829	3.760 ± 0.003	8.90	8.81 ± 0.02	8.83 ± 0.08	···	···	8.81 ± 0.14
V0636 SCO	DCEP	0.833	4.384 ± 0.001	9.51	···	···	···	···	···
U AQL	DCEP	0.846	3.665 ± 0.002	8.93	8.86 ± 0.07	8.75 ± 0.12	···	···	8.86 ± 0.15
η AQL	DCEP	0.856	1.856 ± 0.001	7.16	7.03 ± 0.09	7.16 ± 0.07	···	···	7.03 ± 0.15
W SGR	DCEP	0.880	2.808 ± 0.001	8.09	6.68 ± 0.16	6.54 ± 0.17	8.27 ± 0.19	8.21 ± 0.19	8.27 ± 0.19
GH LUP	CEP	0.968	4.644 ± 0.006	10.22	10.58 ± 0.04	10.01 ± 0.30	···	···	10.58 ± 0.15
S MUS	DCEP	0.985	3.902 ± 0.001	9.64	9.67 ± 0.04	9.57 ± 0.08	···	···	9.67 ± 0.15
S NOR	DCEP	0.989	4.086 ± 0.002	9.78	9.89 ± 0.02	9.55 ± 0.08	···	···	9.88 ± 0.14
β DOR	DCEP	0.993	1.858 ± 0.001	7.57	7.57 ± 0.03	7.59 ± 0.06	7.54 ± 0.11	7.52 ± 0.11	7.55 ± 0.09
ζ GEM	DCEP	1.006	1.982 ± 0.001	7.73	7.93 ± 0.05	7.78 ± 0.06	7.81 ± 0.14	7.78 ± 0.14	···
X CYG	DCEP	1.215	3.680 ± 0.001	10.12	10.26 ± 0.02	10.08 ± 0.06	···	···	10.27 ± 0.14
Y OPH	DCEPS	1.234	2.509 ± 0.001	8.73	8.70 ± 0.03	8.74 ± 0.08	···	···	8.69 ± 0.15
VY CAR	DCEP	1.277	4.527 ± 0.006	11.33	11.19 ± 0.03	10.67 ± 0.07	···	···	11.26 ± 0.34
SW VEL	DCEP	1.370	5.064 ± 0.003	12.04	12.04 ± 0.03	11.60 ± 0.06	···	···	12.04 ± 0.14
T MON	DCEP	1.432	3.422 ± 0.001	10.58	10.59 ± 0.03	10.26 ± 0.06	···	···	10.66 ± 0.40
AQ PUP	DCEP	1.479	4.889 ± 0.004	12.27	12.53 ± 0.04	12.38 ± 0.10	···	···	12.40 ± 0.63
ℓ CAR	DCEP	1.551	0.720 ± 0.001	8.48	8.57 ± 0.02	8.20 ± 0.06	8.56 ± 0.22	8.48 ± 0.22	8.57 ± 0.13
U CAR	DCEP	1.589	3.187 ± 0.006	11.09	10.74 ± 0.03	10.73 ± 0.07	···	···	10.87 ± 0.61
RS PUP	DCEP	1.617	3.316 ± 0.001	11.13	11.29 ± 0.04	10.98 ± 0.10	···	···	11.29 ± 0.15

[a] Sources of the distance modulus μ: $N12$ = Ngeow (2012) with an uncertainty of 0.08 mag; $S11$ = Storm et al. (2011); $G13$ = Groenewegen (2013); LKH = parallax distances with LKH corrections taken from *Hipparcos* (for α UMi & DT Cyg, van Leeuwen 2007) or *HST* (for the rest of Cepheids, Benedict et al. 2007) as listed in Monson et al. (2012, with updated values for β Dor & W Sgr), where LKH corrections for α UMi & DT Cyg are adopted from van Leeuwen (2007); $noLKH$ = parallaxes distances without LKH corrections; $B15$ = Bhardwaj et al. (2015b).

2.1. *The Adopted Distance Moduli*

Since the work of Marengo et al. (2010), new distance moduli for the Cepheids listed in Table 2 have been available from various sources in the literature. These measurements are based on the distance moduli calculated from using a Period-Wesenheit relation as presented in Ngeow (2012); variants of Baade-Wesselink-type infrared surface brightness (IRSB) methods (Storm et al. 2011; Groenewegen 2013); updated parallaxes from *Hipparcos* (van Leeuwen et al. 2007; van Leeuwen 2007) and *Hubble Space Telescope* (*HST*, Benedict et al. 2007; Monson et al. 2012); and a compilation of various distance measurements available in the literature in recent years (Bhardwaj et al. 2015b). Distance moduli from these sources were listed in Table 2. It is worth mentioning that these distance moduli are not all independent of each other, and hence we have applied them separately to derive the absolute magnitudes for our sample of Galactic Cepheids in the next section.

Ngeow (2012) demonstrated that the distance to Galactic Cepheids can be obtained via $\mu_W = I_c - 1.55(V - I_c) + 3.313 \log P + 2.693$, which is based on a calibrated Period-Wesenheit relation. The slope of this Period-Wesenheit relation was derived from a large number of Cepheids in the LMC (Ngeow et al. 2009), and almost identical to the one based on the SMC Cepheids (Ngeow et al. 2015). The intercept of the Period-Wesenheit relation, on the other hand, was calibrated using parallaxes from the *HST* (Benedict et al. 2007). Since μ_W only depends on the pulsation period P and mean magnitudes in the VI_c bands, and as these quantities can be measured with negligible errors for Galactic Cepheids, a constant uncertainty of 0.08 mag is adopted for μ_W (for more details, see Ngeow 2012).

The data sets and methodologies used in deriving the two distance moduli based on the IRSB methods are very similar. The largest difference between them is the adopted period-projection factor (P-p) relation: Storm et al. (2011) used $\mathrm{p} = 1.550 - 0.186 \log P$ while Groenewegen (2013) preferred $\mathrm{p} = 1.50 - 0.24 \log P$. Note that the P-p relation is still a dominant systematic error in the IRSB methods (for a quick overview of the projection factor on Cepheids, see Nardetto et al. 2014, and reference therein), and the uncertainty of the P-p relation directly translates to the uncertainty in the derived IRSB distance. Since the goal of this paper is not to evaluate which P-p relation is a better relation, we leave it to readers to select their own preference.

For the 10 Cepheids with parallaxes listed in Table 2, we did not take an average of the parallaxes from *Hipparcos* and *HST* for the common Cepheids. The parallaxes for α UMi and DT Cyg were adopted from *Hipparcos*, and parallaxes for 8 other Cepheids were taken from *HST* measurements. Following Monson et al. (2012), when fitting the P-L relations for Cepheids with parallaxes we included the cases with and without the Lutz-Kelker-Hanson (LKH, Lutz & Kelker 1973; Hanson 1979) corrections (for further discussion on LKH correction, see Sandage & Saha 2002; Smith 2003, and reference therein). Even though the majority of the work in the literature has included LKH corrections, there are examples of investigations where LKH corrections were not applied (Feast & Catchpole 1997).

Bhardwaj et al. (2015b) compiled a list of Galactic Cepheids with measured distances from the literature, including *HST* parallaxes, the two Baade-Wesselink type IRSB techniques mentioned previously (Storm et al. 2011; Groenewegen 2013), and distances based on main-sequence (MS) fitting to open clusters that hosted Cepheids (Turner 2010). Since the two IRSB distances are not independent of each other, Bhardwaj et al. (2015b) adopted the distances from Storm et al. (2011) as the main source of IRSB distances, or those from Groenewegen (2013) if the former one is not available. A weighted mean was taken if a Cepheid has more than one distance measurement from *HST* parallaxes, IRSB techniques, and MS fitting.

In this paper, we exclude MS fitting distances, such as those given in Turner (2010), for the following reasons. The main concern with MS fitting distances is that the majority of the Cepheid host open clusters were treated separately and individually. As a result, there was a mixture of data quality with a variety of analysis techniques (such as different photometric systems and filters used, the adopted extinction law, cluster memberships that were used to define the main sequence, the assumption of the distance to the Pleiades[9] that calibrates isochrone fitting, the probability of the Cepheid belonging to the open cluster, etc.). For example, the distances to a number of open clusters listed in Turner (2010) and Groenewegen (2013) were based on earlier work in the optical UBV bands, while others included recent investigations in the near infrared JHK_s bands. This heterogeneity suggests that each open cluster could have its own systematic errors, and the overall systematic uncertainty associated with MS fitting distances is difficult to quantify. Some other problems associated with the MS fitting distances were also discussed in Feast (2003). An example is the measured distance modulus to the open cluster Lyngå 6, the host of TW Nor, which could have a wide range of values in the literature[10]. Based on the 13 common Cepheids (2 of them being the DCEPS type) in Turner (2010) and Table 2, the dispersion of the fitted P-L relation (using the same code as described in the next section) is found to be ~ 0.42 mag, which is unreasonably high. After removing TW Nor,which exhibits the largest deviation from the fitted P-L relation, the resulting P-L dispersion of ~ 0.30 mag is still higher than the P-L dispersions discussed in Section 3.1. This suggests that some of the MS fitting distances are not that well constrained. Nevertheless, readers can derive their own MS fitting-based P-L relation using the 24μm photometry in Table 2 based on their preferred MS fitting distances.

2.2. *The Issue of Extinction*

[9] For an overview of the "Pleiades distance controversy," see Melis et al. (2014)

[10] Values of the distance modulus for Lyngå 6 range from $\sim 11.95 \pm 0.51$ (UBV band; Madore 1975, assume $R_V = 3.1$), 11.51 ± 0.08 (BVI_c band; An et al. 2007, this value itself is an average of 11.60 ± 0.11 with BV-band data and 11.42 ± 0.12 with VI_c-band data), 11.41 ± 0.11 (JHK_s band; Majaess et al. 2011), 11.33 ± 0.18 Hoyle et al. (UBV band; 2003), 11.15 ± 0.30 (BVI band; Walker 1985, this value itself is an average of 11.2 with BV-band data and 11.0 with VI_c-band data), 10.8 ± 0.6 (UBV band; van den Bergh & Harris 1976), ~ 10.67 ($ubvy\beta$ band; Kaltcheva 2009) to 10.6 ± 0.3 ($ubvy\beta$ band; Schmidt 1983).

As in Marengo et al. (2010), we ignore extinction because it is expected to be negligible at 24μm. Assuming that the Cardelli et al. (1989) extinction law is valid at 24μm, then at this wavelength the expected value of $A_{24\mu\mathrm{m}}/A_V$ is ~ 0.0024 for $R_V = 3.1$. In the case that the color excess is $E(B-V) = 1.0$, the expected extinction at 24μm is $A_{24\mu\mathrm{m}} = 0.007$ mag. In our combined sample, there are 8 Cepheids with $E(B-V) > 1.0$, and the largest $E(B-V) = 1.568$ for V470 Sco has an extinction of $A_{24\mu\mathrm{m}} = 0.012$ mag (i.e., smaller than the typical errors in distance moduli listed in Table 2). The average $E(B-V) = 0.541$ for our combined sample implies a mean extinction of $A_{24\mu\mathrm{m}} = 0.004$ mag, which can be safely ignored.

In terms of observations, two studies reported the empirical extinction law $A_{24\mu\mathrm{m}}/A_{K_s}$. Flaherty et al. (2007) determined $A_{24\mu\mathrm{m}}/A_{K_s} = 0.46 \pm 0.04$ based on the averaged values of two nearby star-formation regions: Serpens and NGC 2068/2071 (they adopted $A_H/A_{K_s} = 1.55 \pm 0.08$ which is consistent with a value of 1.54 based on the extinction law from Cardelli et al. 1989). Their extinction law is $\sim 22\times$ higher than the expected value of $A_{24\mu\mathrm{m}}/A_{K_s} = 0.021$ from the Cardelli et al. (1989) extinction law, and hence the expected extinction of $A_{24\mu\mathrm{m}}$ will be increased by the same proportion. Nevertheless, the Flaherty et al. (2007) results are based on a small number of sources used to determine the extinction law at 24μm. Depending on the A_{K_s} bins, Chapman et al. (2009) found that $A_{24\mu\mathrm{m}}/A_{K_s}$ ranges from 0.34 ± 0.13 to 1.08 ± 0.32 based on multi-band observations of three molecular clouds (Ophiuchus, Perseus, and Serpens). However, the authors cautioned the unexpected anti-correlation between A_{K_s} and $A_{24\mu\mathrm{m}}/A_{K_s}$ and the large values of $A_{24\mu\mathrm{m}}/A_{K_s}$, which could due to a combination of small number of sources and/or incorrect assumptions by the averaged stellar models used in the fitting. We should emphasize that the determinations of $A_{24\mu\mathrm{m}}/A_{K_s}$ in Flaherty et al. (2007) and Chapman et al. (2009) were obtained in rather "special" places in our Galaxy – either star-formation regions and/or the molecular clouds. These places certainly do not represent the typical environment of our Galaxy. As pointed out by Chapman et al. (2009), "the extinction law at 24μm is not well understood," and therefore we did not apply these empirical extinction laws in this paper.

3. THE PERIOD-LUMINOSITY RELATION

Figure 3 presents the 24μm P-L relations for both the Marengo and MIPSGAL samples with the six adopted distance moduli as mentioned in the previous section. We excluded W Sgr when converting the apparent magnitudes to absolute magnitudes when using the distance moduli from Storm et al. (2011), because this Cepheid exhibits a discrepant distance modulus from Storm et al. (2011) as compared to other independent measurements (Ngeow 2012). W Sgr is known to be a binary or triple system (for example, see Benedict et al. 2007; Evans et al. 2009, 2015, and reference therein). The multiplicity nature of this Cepheid could affect the measurements of its photometric light curve and/or the radial velocity curve (e.g., due to contamination from the companion). This could affect the derived IRSB distance. In fact, W Sgr was eliminated in Storm et al. (2011)'s analysis of the projection-factor relation and their derived P-L relations. Similarly, we removed W Sgr, FF Aql, and DT Cyg when applying the distance moduli taken from Groenewegen (2013). These Cepheids appeared as outliers in Figure 3. Similarly to W Sgr, FF Aql is also a binary system (for example, see Benedict et al. 2007; Groenewegen 2013; Evans et al. 2015, and reference therein). Furthermore, mode identification in FF Aql is still controversial: some authors have adopted a fundamental mode pulsation for this Cepheid (such as in Benedict et al. 2007; van Leeuwen et al. 2007; Marengo et al. 2010) with supporting evidence from Gallenne et al. (2012) and Turner et al. (2013), while others argue that it should be pulsating in the first overtone (for examples, see Antonello et al. 1990; Feast & Catchpole 1997; Kienzle et al. 1999; Storm et al. 2011). Following Marengo et al. (2010), we adopted a fundamental mode pulsation (DCEP type) for FF Aql in Table 2. If this Cepheid is a first overtone pulsator, then its fundamentalized period would be $\log P = 0.806$, bringing it closer to the fitted P-L relation. For first overtone (DCEPS type) Cepheid DT Cyg, its period listed in Table 2 ($\log P = 0.550$) has already been fundamentalized. Using its observed period at $\log P = 0.398$ would place DT Cyg even further from the fitted P-L relation.

When fitting the P-L relation, we used all of the types of Cepheids as listed in the second column of Table 2 and excluded the first overtone DCEPS Cepheids. We did not fit the P-L relation for DCEPS Cepheids only due to their smaller sample size. Since the Cepheid P-L relation is expected to exhibit an intrinsic dispersion, we employed the BCES algorithm (Bivariate, Correlated Errors, and intrinsic Scatter, Akritas & Bershady 1996), implemented in a `python` code `lnr`[11], to fit the P-L relation. The errors in the absolute magnitudes of our Cepheids in the combined sample are a quadratic sum of the photometric errors and errors from distance moduli as listed in Table 2. Other error terms (such as errors

Table 3
Fitted P-L Relations by using Various Distance Moduli.[a]

Source of μ	N	η	β	σ	σ_{int}
All Types					
μ_{N12}	65	-3.16 ± 0.09	-2.48 ± 0.09	0.20	0.19
μ_{S11}	38	-3.29 ± 0.09	-2.45 ± 0.11	0.23	0.22
μ_{G13}	38	-3.07 ± 0.11	-2.58 ± 0.12	0.23	0.22
μ_{LHK}	10	-3.50 ± 0.11	-2.32 ± 0.11	0.12	0.09
μ_{noLKH}	10	-3.52 ± 0.07	-2.26 ± 0.08	0.11	0.08
μ_{B15}	41	-3.29 ± 0.09	-2.43 ± 0.10	0.24	0.23
Exclude DCEPS					
μ_{N12}	58	-3.18 ± 0.10	-2.46 ± 0.10	0.21	0.20
μ_{S11}	34	-3.36 ± 0.09	-2.37 ± 0.11	0.23	0.22
μ_{G13}	36	-3.08 ± 0.12	-2.57 ± 0.13	0.24	0.23
μ_{LHK}	8	-3.56 ± 0.10	-2.27 ± 0.12	0.13	0.11
μ_{noLKH}	8	-3.51 ± 0.09	-2.27 ± 0.11	0.13	0.11
μ_{B15}	37	-3.36 ± 0.09	-2.36 ± 0.11	0.24	0.23

[a] The P-L relation takes the form of $M_{24\mu\mathrm{m}} = \eta \log P + \beta$. σ is the dispersion of the fitted P-L relation, while σ_{int} is the estimated intrinsic dispersion after removing the contribution from random phase photometry. N is the number of Galactic Cepheids used to derive the corresponding P-L relations.

[11] `http://home.strw.leidenuniv.nl/~sifon/pycorner/bces/`

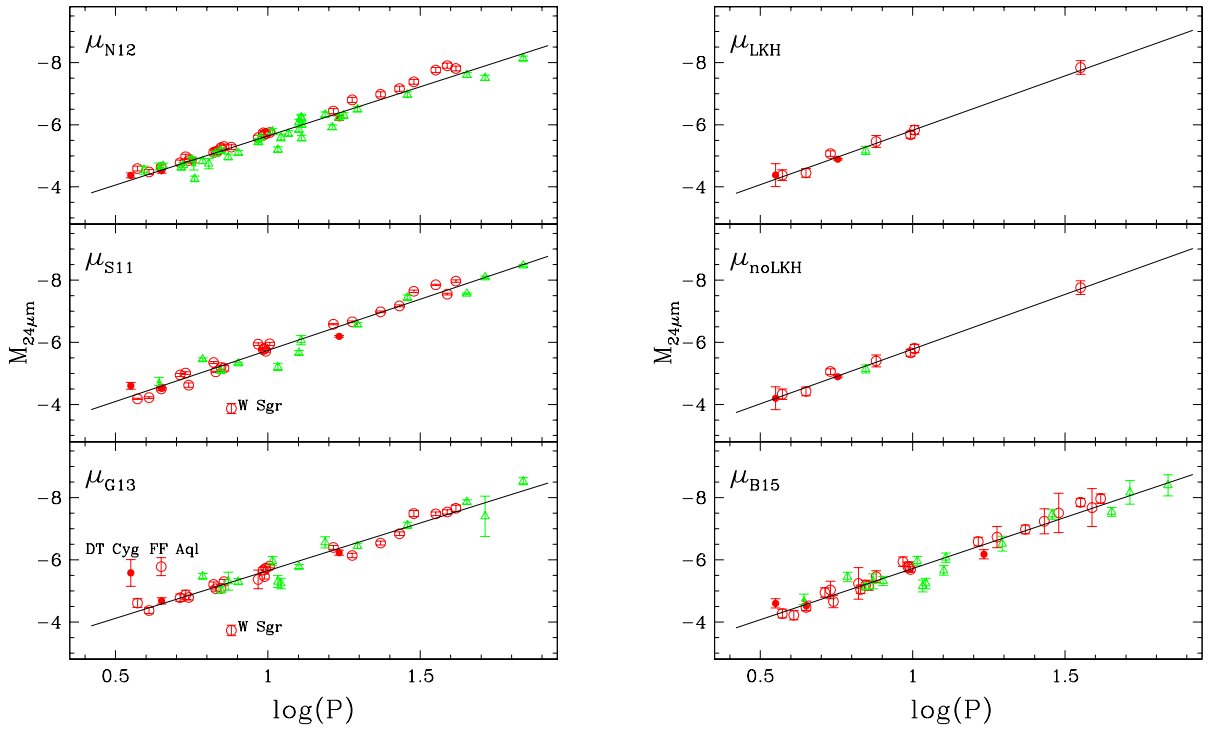

Figure 3. The P-L relation based on Cepheids given in Table 2. Green circles and red triangles represent the Marengo sample and the MIPS sample, respectively. Open symbols are for DCEP- or CEP-type Cepheids, while the filled symbols are for DCEPS-type Cepheids. Labels for adopted distance moduli are the same as in Table 2. Straight lines are fitted P-L relations using all of the types of Cepheids as given in Table 3. Outliers that are not used in the fitting are labeled in the left panel.

for pulsation periods, as they are adopted from literature which generally do not report these errors) are assumed to be negligible. The fitted P-L relations with the six different sources of distance moduli are summarized in Table 3, and shown as straight lines in Figure 3. For a give source of distance moduli, Table 3 implies that the P-L relations derived using either all types of Cepheids or excluding DCEPS are consistent with each other: this is not a surprise given the small number of DCEPS Cepheids in the combined sample.

3.1. *The Scatter of the P-L Relation*

The P-L relation for Cepheids is expected to exhibit an intrinsic dispersion due to the finite width of the instability strip in the color-magnitude diagram (for example, see Madore & Freedman 1991). The *observed* dispersions of the fitted P-L relations, calculated as $\sigma = \sqrt{SSE/(N-2)}$, where $SSE = \sum_{i=1}^{N}(m_i - \eta \log P_i - \beta)^2$, are listed in the fifth column of Table 3. Since the single-epoch 24μm photometry listed in Table 2 was taken during random phases such that $\phi \in [0,1]$ (where ϕ is pulsational phase after folding with period), the observed dispersion σ should include the contribution from the random phase observations after scaling with amplitude (Freedman et al. 2008). For a uniform distribution with boundaries at $x \in [a,b]$, it is well-known that the variance is $(b-a)^2/12$. Assuming that the random phase observations follow a uniform distribution with $\phi \in [0,1]$, and that the observed dispersion σ can be represented as a quadratic sum of the intrinsic dispersion $\sigma_{\rm int}$ and the contribution of random phase observations, then $\sigma_{\rm int} = [\sigma^2 - A^2/12]^{1/2}$, where A is the expected peak-to-peak full amplitude at 24μm (Freedman et al. 2008). An estimate of the expected peak-to-peak full amplitude for the combined sample is given in the Appendix and is found to be $A = 0.26$. Therefore, it is expected that $\sigma_{\rm int} \sim \sigma$ because $A^2/12 \sim 6 \times 10^{-3}$. The calculated $\sigma_{\rm int}$ was listed in the last column of Table 3.

The observed P-L dispersions or intrinsic dispersions listed in Table 3 can be roughly divided into two groups: those around $\sim$ 0.2 mag and $\sim$ 0.1 mag. The former group includes those P-L relations calibrated with distance moduli adopted from Ngeow (2012), Storm et al. (2011), Groenewegen (2013), and Bhardwaj et al. (2015b). The $\sim$ 0.2 mag dispersion found in this group is larger than the expected P-L dispersion in the mid-infrared, suggesting that the dispersion is dominated by the precision and accuracy of the distance to individual Galactic Cepheids. Note that the extra dispersion induced from single-epoch random phase observations for this group is of the order of $\sim 5\%$, and hence cannot account for the $\sim$ 0.2 mag dispersion. On the other hand, P-L relations derived using accurate parallax measurements from *HST* and *Hipparcos* show a dispersion of $\sim$ 0.1 mag. Assuming that the dispersions of P-L relations are similar in both of the IRAC and MIPS bands, then the above dispersion is closer to the expected value of $\sim$ 0.1 mag based on the IRAC-band P-L relations derived from Cepheids in our Galaxy (Monson et al. 2012; Ngeow 2012) and in the LMC (Madore et al. 2009; Ngeow et al. 2009; Scowcroft et al. 2011). Extra contribution due to single-epoch random phase observations on the P-L dispersion, on the other hand, can vary from $\sim 20\%$ to $\sim 40\%$ in this group and

should be closer to reality.

3.2. *Testing the Consistency of the P-L Relations Derived with Different Distance Moduli*

Inspecting Table 3 reveals that the slopes (η) of the fitted P-L relations range from -3.07 ± 0.11 to -3.52 ± 0.07 when using all types of Cepheids and from -3.08 ± 0.12 to -3.56 ± 0.10 after excluding DCEP Cepheids, which represent a difference of ~ 0.5 mag/dex. Similarly, the intercepts (β) of the fitted P-L relations show a difference of ~ 0.3 mag when adopting different sources of distance moduli. For example, P-L relations using the distance moduli from Groenewegen (2013) have the shallowest P-L slopes and brightest P-L intercepts. In contrast, P-L relations that are based on the parallaxes from *HST* and *Hipparcos* provide the steepest P-L slopes and faintest P-L intercepts. On the other hand, the P-L relations obtained using the distance moduli from Storm et al. (2011) and Bhardwaj et al. (2015b) are almost identical to each other, as the compilation of distance moduli given in Bhardwaj et al. (2015b) was dominated by the former source. As in our previous work, we apply the standard statistical t-test to test the consistency of these P-L slopes and intercepts. Simply speaking, we calculated the T-values for an estimator $\hat{W}$ ($=\eta$ or β) for two linear regressions with sample sizes of n and m as $T = |\hat{W}_n - \hat{W}_m|/\sqrt{\mathrm{Var}(\hat{W}_n) + \mathrm{Var}(\hat{W}_m)}$, where $\mathrm{Var}(\hat{W})$ is the variance of the estimator $\hat{W}$. Values of $\mathrm{Var}(\hat{\eta})$ and $\mathrm{Var}(\hat{\beta})$ were calculated in the `lnr` code, which we adopted when computing the T-values. We evaluated the expected p-value and the $t_{\alpha/2,\nu}$-value based on the t-distribution with $\nu = n+m-4$ degree of freedom at a confidence level of $\alpha = 0.05$. The null hypothesis of the equivalent $\hat{W}$ can be rejected if $T > t_{\alpha/2,\nu}$ or $p < 0.05$. The t-test results for the P-L slopes (η) and P-L intercepts (β) are summarized in Table 4 and 5, respectively.

Based on the t-test results presented in Table 4, both consistency and inconsistency of the P-L slopes were seen with the six difference sources of distance moduli. The steepest P-L slopes obtained from *HST* and *Hipparcos* parallax measurements without LKH corrections do not agree with all of the other four P-L slopes. If the LKH corrections were applied, then the disagreement of these P-L slopes still exists when compared to the P-L slopes by using the distance moduli from either Ngeow (2012) or Groenewegen (2013). A similar situation also occurs if DCEPS Cepheids are excluded. When using the distance moduli from *HST* and *Hipparcos*, the fitted P-L relations gave the steepest P-L slopes (either with or without LKH corrections), despite the very accurate parallax measurements. We suspected this to be caused by the small number of Cepheids in the sample, especially as there is only one Cepheid (ℓ Car) beyond the 10 days period. We test this assumption in the next sub-section. In terms of the P-L intercepts, Table 5 reveals that only one pair of P-L intercepts do not agree with each other.

3.3. *Tests of Steep P-L Slopes from Small Number of Samples*

As mentioned previously, we suspect that the steep P-L slopes based on μ_{LKH} (and/or μ_{noLKH}), as presented in Table 3, are due to the small numbers of Cepheids in the sample (i.e. 10 Cepheids, or 8 after excluding DCEPS Cepheids). Furthermore, there's only one long period Cepheid in the sample, which might bias the fitting of the P-L relation. To test this, we used the sample of 65 Cepheids with distance moduli from Ngeow (2012, i.e. μ_{N12}), referred to as the parent sample in our tests, and only selected the 10 Cepheids that are common to the sample with *HST* and *Hipparcos* parallaxes (hereafter the parallax sample). The fitted P-L slope for this sub-sample is -3.32 ± 0.15, which is steeper than the P-L slope from the parent sample of -3.16 ± 0.09. We also created simulated data by randomly selecting (without replacement) nine Cepheids from the parent sample with $\log P < 1.02$, and one Cepheid in the parent sample within the period range of $1.45 < \log P < 1.65$ to represent ℓ Car, in order to mimic the sample distribution of the 10 Cepheids in the parallax sample. We then fit the P-L relation to these 10 randomly selected Cepheids and repeat this process 2000 times to build up the distribution of the fitted P-L slopes. The left panel of Figure 4 displays such a distribution where the peak occurs at ~ -3.4 to ~ -3.5. Our tests suggested that the sample distribution within the 10 Cepheids in the parallax sample, especially with only one long period Cepheid, could bias the fitted P-L slope to a steeper value. The right panels of Figure 4 show three examples of P-L relations based on the randomly selected 10 Cepheids such that the fitted P-L slopes varied from ~ -3 to ~ -4.

4. DISCUSSION AND CONCLUSION

In this work, we expand the sample of Galactic Cepheids with 24μm photometry from 29, given in Marengo et al. (2010), to 65 after cross-matching known Galactic Cepheids with the MIPSGAL catalog (Gutermuth & Heyer 2015). We adopted six different distance moduli from the literature to calibrate the 24μm P-L relation for these Cepheids, as these distance moduli represent the best measurements to date in the literature since Marengo et al. (2010).

When comparing the six sets of P-L relations, we found that the P-L slopes based on parallax measurements from *HST* and *Hipparcos* (either with or without LKH corrections) do not agree with the other P-L slopes derived from various other means. Our simulation tests suggested that the sampling of these 10 (or less) Cepheids might bias the fitting of P-L slopes. Furthermore, the only long-period Cepheid ℓ Car in this sample was found to be lying toward the red edge of the instability strip (Turner 2010), which could bias the fitting of the P-L relation (i.e., the fitted regression line will not pass through the central region of the instability strip; Majaess 2010). Therefore, we do not recommend using the P-L relations derived from these 10 (or less) Cepheids (i.e. entries with μ_{LKH} and μ_{noLKH} in Table 3). For the remaining four P-L relations, the P-L relations based on the distance moduli from Storm et al. (2011) and Bhardwaj et al. (2015b, ; entries with μ_{S11} and μ_{B15} in Table 3) are essentially identical to each other. Each method used to calibrate the Cepheid distances has their own advantages and disadvantages, and different systematic uncertainties. Yet the following P-L relation is favored: $M_{24\mu\mathrm{m}} = -3.18(\pm0.10)\log P - 2.46(\pm0.10)$, since it is derived from 58 Cepheids calibrated with distance moduli from Ngeow (2012) – the largest sample of Cepheids at this wave-

Table 4
Statistical t-test results for P-L Slopes with Various Sources of Distance Moduli.[a]

	μ_{N12}	μ_{S11}	μ_{G13}	μ_{LKH}	μ_{noLKH}	μ_{B15}
			All Types			
μ_{N12}	···	···	···	···	···	···
μ_{S11}	(1.005,1.984,0.318)	···	···	···	···	···
μ_{G13}	(0.645,1.984,0.520)	(1.549,1.993,0.126)	···	···	···	···
μ_{LHK}	**(2.429,1.994,0.018)**	(1.522,2.015,0.135)	**(2.813,2.015,0.007)**	···	···	···
μ_{noLKH}	**(3.124,1.994,0.003)**	**(2.019,2.015,0.049)**	**(3.430,2.015,0.001)**	(0.118,2.120,0.908)	···	···
μ_{B15}	(1.016,1.983,0.312)	(0.001,1.992,0.999)	(1.563,1.992,0.122)	(1.539,2.012,0.130)	**(2.053,2.012,0.046)**	···
			Exclude DCEPS			
μ_{N12}	···	···	···	···	···	···
μ_{S11}	(1.285,1.987,0.202)	···	···	···	···	···
μ_{G13}	(0.639,1.987,0.524)	(1.843,1.997,0.070)	···	···	···	···
μ_{LHK}	**(2.600,1.999,0.012)**	(1.425,2.024,0.162)	**(3.044,2.021,0.004)**	···	···	···
μ_{noLKH}	**(2.388,1.999,0.020)**	(1.160,2.024,0.253)	**(2.856,2.021,0.007)**	(0.309,2.179,0.762)	···	···
μ_{B15}	(1.311,1.986,0.193)	(0.003,1.996,0.997)	(1.873,1.995,0.065)	(1.448,2.020,0.155)	(1.179,2.020,0.245)	···

[a] Values in parentheses are $(T, t_{\alpha/2,\nu}, p-\text{value})$. The bold-faced entries indicate that the null hypothesis of the equivalent P-L slopes can be rejected.

Table 5
Statistical t-test results for P-L Intercepts with Various Sources of Distance Moduli.[a]

	μ_{N12}	μ_{S11}	μ_{G13}	μ_{LKH}	μ_{noLKH}	μ_{B15}
			All Types			
μ_{N12}	···	···	···	···	···	···
μ_{S11}	(0.217,1.984,0.828)	···	···	···	···	···
μ_{G13}	(0.709,1.984,0.480)	(0.858,1.993,0.394)	···	···	···	···
μ_{LHK}	(1.077,1.994,0.285)	(0.805,2.015,0.425)	(1.601,2.015,0.117)	···	···	···
μ_{noLKH}	(1.773,1.994,0.080)	(1.391,2.015,0.171)	**(2.218,2.015,0.032)**	(0.467,2.120,0.647)	···	···
μ_{B15}	(1.303,1.983,0.763)	(0.074,1.992,0.941)	(0.942,1.992,0.349)	(0.748,2.012,0.458)	(1.344,2.012,0.185)	···
			Exclude DCEPS			
μ_{N12}	···	···	···	···	···	···
μ_{S11}	(0.587,1.987,0.559)	···	···	···	···	···
μ_{G13}	(0.674,1.987,0.502)	(1.181,1.997,0.242)	···	···	···	···
μ_{LHK}	(1.175,1.999,0.244)	(0.585,2.024,0.562)	(1.699,2.021,0.097)	···	···	···
μ_{noLKH}	(1.190,1.999,0.238)	(0.593,2.024,0.557)	(1.716,2.021,0.094)	(0.001,2.179,0.999)	···	···
μ_{B15}	(0.676,1.986,0.501)	(0.070,1.996,0.944)	(1.271,1.995,0.208)	(0.531,2.020,0.598)	(0.538,2.020,0.594)	···

[a] Values in parentheses are $(T, t_{\alpha/2,\nu}, p-\text{value})$. The bold-faced entries indicate the null hypothesis of the equivalent P-L intercepts can be rejected.

length after excluding DCEPS. This P-L relation carries an observed dispersion of 0.21 mag, or an intrinsic dispersion of 0.20 mag after removed the estimated contribution from random phase observations. The slope of that P-L relation lies between that inferred from the distance moduli cited in Groenewegen (2013) and Storm et al. (2011) or Bhardwaj et al. (2015b). Compared to the P-L relations listed in Table 1, the slope of our favored P-L relation is shallower and the P-L intercept is consistent with those taken from Ngeow (2012). Finally, our favored P-L relation remained unchanged if extinction corrections using the Cardelli et al. (1989) extinction law were included in the fitting.

Since the radial variations, rather than the temperature variations, will dominate the luminosity variations for Cepheids in longer wavelengths, the slopes of the P-L relations are expected to approach an asymptotic value in the mid-infrared (Madore & Freedman 1991; Freedman et al. 2008; Freedman & Madore 2010; Scowcroft et al. 2011; Madore & Freedman 2012). Following the prescription outlined in Neilson et al. (2010) and Ngeow et al. (2012b), the mid-infrared P-L relation can be written as $M_{MIR} = (-5\times a_R - 2.5\times a_{T_{eff}})\log P +$ constant, where a_R is the slope of the period-radius relation. The term $a_{T_{eff}}$ represents the slope of the period-temperature relation due to the Rayleigh-Jean tail of the black-body radiation. By using the $(V-I)_0$ period-color relation from Tammann et al. (2003), together with the temperature-color conversion given in Neilson et al. (2010), we have $-2.5 \times a_{T_{eff}} = 0.175$. Therefore, the predicted slope of the mid-infrared P-L relation is $-5 \times a_R + 0.175$, where a_R ranges from 0.680 ± 0.017 (Gieren et al. 1999) to 0.750 ± 0.024 (Gieren et al. 1998), which roughly bracket the existing values in literature. In Figure 5, the slopes of the multi-band P-L relations for Galactic Cepheids, including the 24μm band, were plotted as a function of the wavelengths. Together with the P-L slopes in the IRAC bands, our 24μm-band P-L slope implies that a_R should be a lower value.

In the near future, *Gaia* will provide precise and accu-

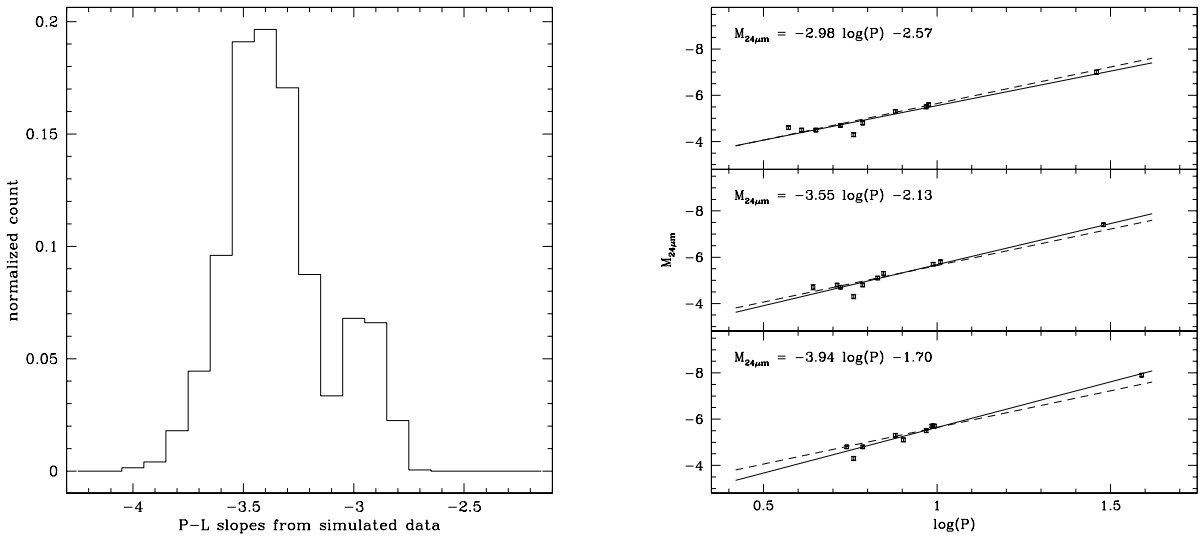

Figure 4. Left panel: distribution of the P-L slopes based on simulated data (see text for more details). **Right panel:** simulated P-L relations for three randomly selected cases. The squares are data points that randomly drawn from the parent sample to mimic the 10 data points for the case of using distance moduli based on *HST* and *Hipparcos*. Solid and dashed lines are the fitted P-L relations from the simulated data and from the parent sample, respectively.

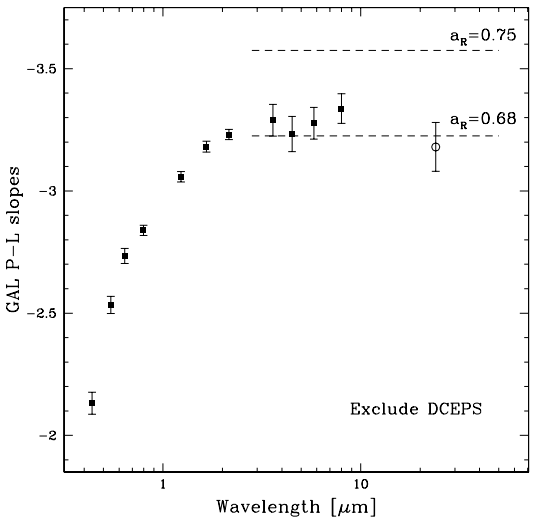

Figure 5. Slopes of the P-L relations as a function of wavelength for Galactic Cepheids (after excluding DCEPS Cepheids). Filled squares are the P-L slopes taken from Ngeow (2012), while the open circle represents the slope of our favored 24μm P-L relation. All of these P-L relations were derived using the same distance moduli presented in Ngeow (2012). The two dashed horizontal lines are the predicted P-L slopes in the mid-infrared based on different slopes of the period-radius relation a_R (see the text for more details).

rate parallaxes to most of the Cepheids listed in Table 2, as well as other Galactic Cepheids. We also anticipate that *JWST* will be able to observe a large number of Galactic Cepheids in the mid-infrared. Hence, we expect that a better-calibrated mid-infrared P-L relation will be available soon by combining the data from *Gaia* and *JWST*, which can be applied to extra-galactic Cepheids for distance scale applications. The distances derived from the 24μm P-L relation can be used to serve as a cross-check with other distances based on period-Wesenheit relations or the mid-infrared P-L relations at 3.6μm that have comparable dispersions. For a Cardelli et al. (1989)-type extinction law, the distance modulus in 24μm ($\mu_{24\mu m}$) will be approximately the same as the true distance modulus because the extinction is negligible as λ^{-1} approaches zero. Rich et al. (2014) demonstrated how is the true distance modulus μ_0 and color excess $E(B-V)$ can be derived for a galaxy by using the distance moduli μ_λ derived from multi-wavelength P-L relations on the plot of μ_λ versus λ^{-1}. Including an additional data point at 24μm could assist in constraining the μ_0 and $E(B-V)$. On the other hand, outliers in the 24μm P-L relation could hint that the 24μm photometry of those Cepheids suffered from a different extinction law at this wavelength (such as these Cepheids being located near a star-formation region).

We thank the referee for valuable input which improved the manuscript. CCN acknowledges the funding from the Ministry of Science and Technology (Taiwan) under the contract 101-2112-M-008-017-MY3 and 104-2112-M-008-012-MY3. SS thanks Dr. Chow-Choong Ngeow for this brilliant opportunity to visit IANCU as a summer intern, and for suggesting this highly intriguing project to work on and guiding him through it. SS thanks Dr. Kaushar Vaidya for introducing him to IANCU and the field of Astronomy. SS thanks Dr. Wen-Ping Chen and other faculty for the highly stimulating discussions, and the entire staff and students of the institute for making the stay at the institute comfortable. AB acknowledges the Senior Research Fellowship grant 09/045(1296)/2013-EMR-I from Human Resource Development Group (HRDG), which is a division of Council of Scientific and Industrial Research (CSIR), India. Part of this work is supported by the grant provided by Indo-U.S. Science and Technology Forum under the Joint Center for Analysis of Variable Star Data. This research has made use of (a) the NASA/IPAC Infrared Science Archive, which is operated by the Jet Propulsion Laboratory, California Institute of Technology, under contract with the National Aeronautics and Space Administra-

tion, and (b) the SIMBAD database, operated at CDS, Strasbourg, France.

APPENDIX

ESTIMATING THE 24μM AMPLITUDES FOR GALACTIC CEPHEIDS IN OUR SAMPLE

Since the 24μm photometry was taken at random phases of the pulsation cycles, it is necessary to estimate the peak-to-peak amplitudes of the Cepheids in the combined sample at 24μm in order to evaluate the intrinsic dispersion of the derived P-L relation (Freedman et al. 2008; Madore et al. 2009). To estimate the expected amplitudes at 24μm for the Galactic Cepheids in the combined sample, we collected their amplitudes in the $UBVR_cI_c$-band from Klagyivik & Szabados (2009). Furthermore, their amplitudes in the JHK band and the mid-infrared 3.6 and 4.5μm bands were augmented from Bhardwaj et al. (2015a) based on the fitting of a Fourier expansion to the observed light curves data. Note that the only available full light curve data in the mid-infrared is for the 3.6μm and 4.5μm bands (Monson et al. 2012), which can be used to estimate the amplitudes in these two bands. Also, not all of the Galactic Cepheids in the combined sample have amplitudes in all of the available bands. For each Cepheids in our sample, the amplitudes in each bands (Amp_λ) were normalized with the V-band amplitudes (Amp_V). We then took the average of the amplitude ratio ($\mathrm{Amp}_\lambda/\mathrm{Amp}_V$) at a given bandpass λ after removing the 3σ outliers. The upper panel of Figure 6 presents the averaged amplitude ratios (and their associated standard deviations) from the U band to 4.5μm band, which shows that the amplitude ratios asymptotically decreased from the U band to the infrared bands. This is because the temperature and radius variations contribute to the overall amplitude variation in the optical bandpasses. For bandpasses in the near- and mid-infrared, it is expected that the amplitude variation will only be caused by radius variation, and hence the amplitude ratio should approach a constant value. We fit the amplitude ratios in the upper panel of Figure 6 with a piecewise function such that a polynomial function was used to fit the amplitude ratios with $\lambda < \lambda_c$, and a constant term for those with $\lambda > \lambda_c$. Since the polynomial function created numerical "bumps" or "wiggles" near λ_c, after trial and error we have picked $\lambda_c \sim 1.25\mu$m such that these numerical bumps are minimized and the curves are well fit to the data points. The lower panel of Figure 6 displayed the values of such constant term as a function of λ_c, which remained as a straight horizontal line for $1.10\mu\mathrm{m} < \lambda_c < 1.65\mu\mathrm{m}$. The constant term was found to be 0.34, and hence the expected peak-to-peak amplitude at 24μm is 0.26 given that the mean V-band amplitude is 0.75 for the combined sample.

REFERENCES

Akritas, M. G., & Bershady, M. A. 1996, ApJ, 470, 706
An, D., Terndrup, D. M., & Pinsonneault, M. H. 2007, ApJ, 671, 1640
Antonello, E., Poretti, E., & Reduzzi, L. 1990, A&A, 236, 138
Bhardwaj, A., Kanbur, S. M., Singh, H. P., Macri, L. M., & Ngeow, C.-C. 2015a, MNRAS, 447, 3342
Bhardwaj, A., Kanbur, S. M., Singh, H. P., Macri, L. M., Ngeow, C.-C., Wagner-Kaiser, R. & Sarajedini, A. 2015b, AJ Accepted (arXiv:1510.03682)
Benedict, G. F., McArthur, B. E., Feast, M. W., et al. 2007, AJ, 133, 1810
Bouchet, P., García-Marín, M., Lagage, P.-O., et al. 2015, PASP, 127, 612
Cardelli, J. A., Clayton, G. C., & Mathis, J. S. 1989, ApJ, 345, 245
Carey, S. J., Noriega-Crespo, A., Mizuno, D. R., et al. 2009, PASP, 121, 76
Chapman, N. L., Mundy, L. G., Lai, S.-P., & Evans, N. J., II 2009, ApJ, 690, 496
Evans, N. R., Massa, D., & Proffitt, C. 2009, AJ, 137, 3700
Evans, N. R., Berdnikov, L., Lauer, J., et al. 2015, AJ, 150, 13
Feast, M. W., & Catchpole, R. M. 1997, MNRAS, 286, L1
Feast, M. 2003, Stellar Candles for the Extragalactic Distance Scale, Edited by D. Alloin and W. Gieren, Lecture Notes in Physics, 635, 45
Flaherty, K. M., Pipher, J. L., Megeath, S. T., et al. 2007, ApJ, 663, 1069
Freedman, W. L., Madore, B. F., Gibson, B. K., et al. 2001, ApJ, 553, 47
Freedman, W. L., Madore, B. F., Rigby, J., Persson, S. E., & Sturch, L. 2008, ApJ, 679, 71
Freedman, W. L., & Madore, B. F. 2010, ApJ, 719, 335
Gallenne, A., Kervella, P., Mérand, A., et al. 2012, A&A, 541, A87
Gieren, W. P., Fouqué, P., & Gómez, M. 1998, ApJ, 496, 17
Gieren, W. P., Moffett, T. J., & Barnes, T. G., III 1999, ApJ, 512, 553
Groenewegen, M. A. T. 2013, A&A, 550, A70
Gutermuth, R. A., & Heyer, M. 2015, AJ, 149, 64
Hanson, R. B. 1979, MNRAS, 186, 875
Hoyle, F., Shanks, T., & Tanvir, N. R. 2003, MNRAS, 345, 269
Inno, L., Matsunaga, N., Bono, G., et al. 2013, ApJ, 764, 84
Kaltcheva, N. 2009, PASP, 121, 1326
Kienzle, F., Moskalik, P., Bersier, D., & Pont, F. 1999, A&A, 341, 818
Klagyivik, P., & Szabados, L. 2009, A&A, 504, 959
Lutz, T. E., & Kelker, D. H. 1973, PASP, 85, 573
Madore, B. F. 1975, A&A, 38, 471
Madore, B. F., & Freedman, W. L. 1991, PASP, 103, 933
Madore, B. F., Freedman, W. L., Rigby, J., et al. 2009, ApJ, 695, 988
Madore, B. F., & Freedman, W. L. 2012, ApJ, 744, 132
Majaess, D. 2010, Acta Astronomica, 60, 121
Majaess, D., Turner, D., Moni Bidin, C., et al. 2011, ApJ, 741, L27
Majaess, D., Turner, D. G., & Gieren, W. 2013, ApJ, 772, 130
Marengo, M., Evans, N. R., Barmby, P., et al. 2010, ApJ, 709, 120
Melis, C., Reid, M. J., Mioduszewski, A. J., Stauffer, J. R., & Bower, G. C. 2014, Science, 345, 1029

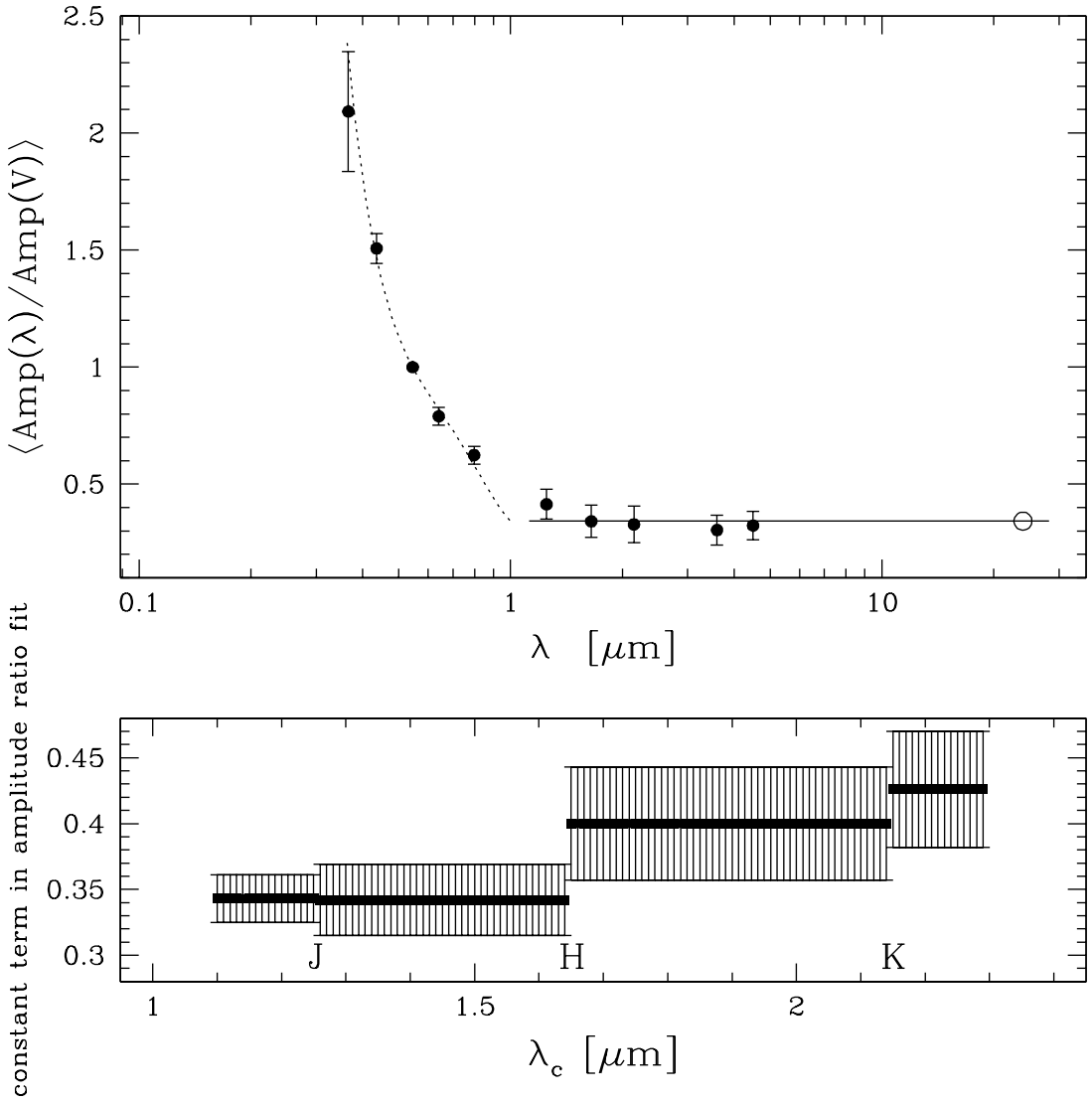

Figure 6. Upper panel: the averaged amplitude ratios as a function of the bandpass λ for the Cepheids in the combined sample. The error bars represent the 1σ standard deviation around the averaged value. By definition, the amplitude ratio in the V band should equal to one with vanished standard deviation. A piecewise function was used to fit the data points (see text for more details), represented by the dotted curves for $\lambda < \lambda_c$ and a straight horizontal line for $\lambda > \lambda_c$. The open circle indicates the expected amplitude ratio at 24μm. **Lower panel:** the value of the constant term in the fitting of piecewise function as a function of λ_c. The λ_c where discontinuities (either in the error bars or the values) occurred corresponding to the central wavelengths in JHK bands.

Monson, A. J., Freedman, W. L., Madore, B. F., et al. 2012, ApJ, 759, 146
Nardetto, N., Storm, J., Gieren, W., Pietrzyński, G., & Poretti, E. 2014, Proceedings of the International Astronomical Union, 9, 145
Neilson, H. R., Ngeow, C.-C., Kanbur, S. M., & Lester, J. B. 2010, ApJ, 716, 1136
Ngeow, C., & Kanbur, S. M. 2008, ApJ, 679, 76
Ngeow, C.-C., Kanbur, S. M., Neilson, H. R., Nanthakumar, A., & Buonaccorsi, J. 2009, ApJ, 693, 691
Ngeow, C.-C., & Kanbur, S. M. 2010, ApJ, 720, 626
Ngeow, C.-C. 2012, ApJ, 747, 50
Ngeow, C.-C., Marconi, M., Musella, I., Cignoni, M., & Kanbur, S. M. 2012a, ApJ, 745, 104
Ngeow, C.-C., Kanbur, S. M., Bellinger, E. P., et al. 2012b, Ap&SS, 341, 105
Ngeow, C.-C., Kanbur, S. M., Bhardwaj, A., & Singh, H. P. 2015, ApJ, 808, 67
Rich, J. A., Persson, S. E., Freedman, W. L., et al. 2014, ApJ, 794, 107
Riebel, D., Boyer, M. L., Srinivasan, S., et al. 2015, ApJ, 807, 1
Rieke, G. H., Young, E. T., Engelbracht, C. W., et al. 2004, ApJS, 154, 25
Rieke, G. H., Wright, G. S., Boker, T., et al. 2015, PASP, 127, 584
Riess, A. G., Macri, L., Casertano, S., et al. 2011, ApJ, 730, 119
Sandage, A., & Saha, A. 2002, AJ, 123, 2047
Sandage, A., Tammann, G. A., Saha, A., et al. 2006, ApJ, 653, 843
Schmidt, E. G. 1983, AJ, 88, 104
Scowcroft, V., Freedman, W. L., Madore, B. F., et al. 2011, ApJ, 743, 76
Smith, H. 2003, MNRAS, 338, 891

Storm, J., Gieren, W., Fouqué, P., et al. 2011, A&A, 534, A94
Tammann, G. A., Sandage, A., & Reindl, B. 2003, A&A, 404, 423
Turner, D. G. 2010, Ap&SS, 326, 219
Turner, D. G., Kovtyukh, V. V., Luck, R. E., & Berdnikov, L. N. 2013, ApJ, 772, L10
van den Bergh, S., & Harris, G. L. H. 1976, ApJ, 208, 765
van Leeuwen, F., Feast, M. W., Whitelock, P. A., & Laney, C. D. 2007, MNRAS, 379, 723
van Leeuwen, F. 2007, A&A, 474, 653
Walker, A. R. 1985, MNRAS, 213, 889